Vacuum 159 (2019) 161–172

Contents lists available at ScienceDirect

Vacuum

journal homepage: www.elsevier.com/locate/vacuum

Time-dependent simulation of the flow reduction of D_2 and T_2 in the KATRIN experiment

F. Friedel[a,*], C. Röttele[a,**], L. Schimpf[a,***], J. Wolf[a], G. Drexlin[a], M. Hackenjos[a], A. Jansen[b], M. Steidl[b], K. Valerius[b]

[a] Institute of Experimental Particle Physics (ETP), Karlsruhe Institute of Technology (KIT), Wolfgang-Gaede-Str. 1, 76131 Karlsruhe, Germany
[b] Institute for Nuclear Physics (IKP), Karlsruhe Institute of Technology (KIT), Hermann-von-Helmholtz-Platz 1, 76344 Eggenstein-Leopoldshafen, Germany

ARTICLE INFO

Keywords:
KATRIN experiment
Cryogenic pump
Pumping speed
Tritium
TPMC simulation

ABSTRACT

The KArlsruhe TRItium Neutrino experiment (KATRIN) aims to measure the effective electron anti-neutrino mass with an unprecedented sensitivity of 0.2 eV/c^2, using β-electrons from tritium decay. Superconducting magnets will guide the electrons through a vacuum beamline from the windowless gaseous tritium source through differential and cryogenic pumping sections to a high resolution spectrometer. At the same time tritium gas has to be prevented from entering the spectrometer. Therefore, the pumping sections have to reduce the tritium flow by at least 14 orders of magnitude. This paper describes various simulation methods in the molecular flow regime used to determine the expected gas flow reduction in the pumping sections for deuterium (commissioning runs) and for radioactive tritium. Simulations with MolFlow+ and with an analytical model are compared with each other, and with the stringent requirements of the KATRIN experiment.

1. Introduction

The **KA**rlsruhe **TRI**tium **N**eutrino experiment (KATRIN) has been designed to determine the effective mass of electron anti-neutrinos with an unprecedented sensitivity of 200 meV/c^2 at 90% confidence level, using electrons from tritium β-decay [1,2]. The analysis is focused on the last few eV below the 18.6 keV endpoint of the β-spectrum.

The experiment is located at the Karlsruhe Institute of Technology (KIT), Campus North, near Karlsruhe, Germany. The approximately 70 m long beamline is shown in Fig. 1. The experiment can be divided into two main sections. The source and transport section is responsible for the production and adiabatic transport of tritium β-particles to the spectrometer and detector section. Their energy is determined in the integrating, electrostatic main spectrometer, which can provide high energy resolution with a wide open solid angle acceptance for β-electrons, emitted isotropically in the Windowless Gaseous Tritium Source (WGTS). The expected signal rate in the last eV of the β-spectrum is about 10^{-2} counts per second; thus, a necessary precondition of reaching the neutrino mass sensitivity goal is a similarly low background rate [1]. This stringent requirement entails a thorough understanding and mitigation of background sources along the entire beamline of the experiment. Of particular importance are background electrons produced in the main spectrometer. One such background source are β-decays of tritium passing from the WGTS through the connecting beamline into the spectrometer.

The WGTS has been designed to produce more than 10^{11} β-particles per second [3]. A constant flow of 95% pure T_2 gas is injected at the center of the 10 m long beam tube with a pressure of 3.4×10^{-3} mbar at a temperature of 30 K [4]. Superconducting magnets adiabatically guide half the emitted electrons through the differential [5] and cryogenic [6,7] pumping sections towards the spectrometer section, while reducing the tritium flow by at least 14 orders of magnitude [1].

Over 99% of the gas is already pumped out by the turbo-molecular pumps (TMP) of the first stages of the differential pumping systems, which are integrated at both ends of the source cryostat (DPS1-R and DPS1-F). The detailed rarefied gas flow simulation has been described by Kuckert et al. [4]. In the remaining text, WGTS refers to the entire source cryostat, including the DPS1-R and DPS1-F subsections. In this paper, we describe the simulation in the molecular flow regime of the flow reduction system, which reduces the remaining tritium flow by another 12 orders of magnitude. The system includes the second stage of the Differential Pumping Section (DPS2-F) designed for a reduction

* Corresponding author.
** Corresponding author.
*** Corresponding author.
E-mail addresses: fabian.friedel@kit.edu (F. Friedel), carsten.roettele@kit.edu (C. Röttele), lutz.schimpf@kit.edu (L. Schimpf).

https://doi.org/10.1016/j.vacuum.2018.10.002
Received 30 July 2018; Received in revised form 21 September 2018; Accepted 1 October 2018
Available online 05 October 2018

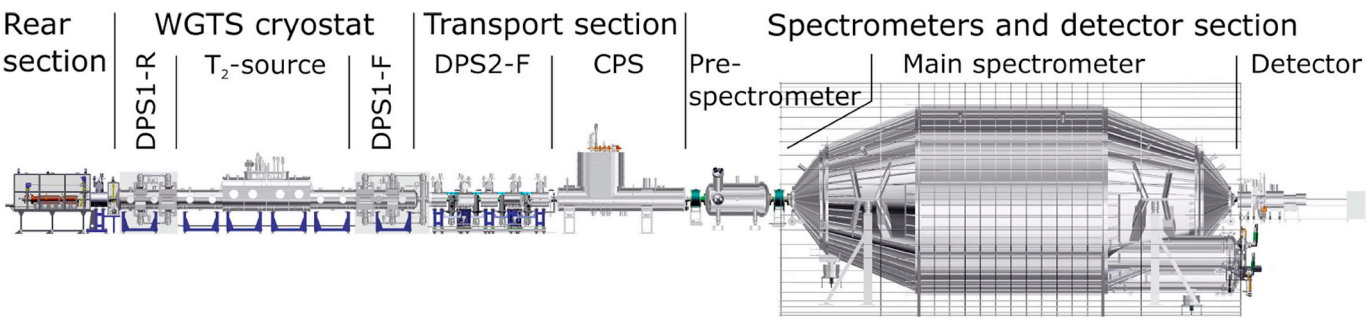

Fig. 1. Overview of the 70 m long KATRIN experiment. Tritium gas is injected in the source (WGTS) and pumped out in adjacent pumping sections (DPS1/2, CPS). Electrons from β-decay are magnetically guided to the electrostatic spectrometers, analyzing their energy, and are counted at the detector.

factor of 10^5, and the Cryogenic Pumping Section (CPS) designed for a reduction factor of at least 10^7.

Section 2 describes the general design and the vacuum system of both pumping systems. The Test Particle Monte Carlo (TPMC) simulation with MolFlow+ [8] is described in Sec. 3. The large flow reduction along the beam tube forced us to subdivide the simulation of a long beam tube into several independent steps and concatenate the results in the subsequent analysis. In the analysis of the CPS simulation the time dependence of the reduction factor was introduced, assuming a slow migration of the adsorbed and redesorbed tritium towards the spectrometer section. An alternative simulation method for the CPS is introduced in Sec. 4. The geometry is hard-coded in C++, optimizing the speed of the simulation. It also allows the simulation of time-dependent properties that are difficult to characterize with MolFlow+ in a single pass. In Sec. 5, the results are presented. The implications of the results and systematic uncertainties, due to some simplifications used in the model, are discussed in Sec. 6.

2. The pumping sections

2.1. The differential pumping section

The differential pumping section (DPS2-F) has to fulfill three different tasks. The first task is to reduce the tritium gas flow between the WGTS and the CPS by 5 orders of magnitude. The second task is to guide the β-electrons adiabatically from the WGTS downstream to the cryogenic pumping section (CPS) along the magnetic flux tube. Each tritium decay in the WGTS ionizes on average about 10 tritium molecules, which are also guided by the magnetic flux tube through the beamline. The third task is to prevent these ions from reaching the spectrometer section, where they would increase the background rate.

2.1.1. Geometry

The DPS2-F has five pump ports (PP0, PP1, …, PP4), which are aligned perpendicular to the interconnecting beamlines (BT1-5) as can be seen in Fig. 2. Pump port 0 was added at a late stage during the design of the pumping section, which is why in previous publications the DPS2-F is mostly described with only four pump ports [9,10]. Incoming and outgoing beamlines of PP1-4 change direction at the pump ports by 20°. This geometry prevents a direct line of sight and increases the number of collisions with the walls, and thus, the pumping probability for the neutral molecules. Electrostatic dipoles (half-pipe-shaped stainless-steel electrodes) and ring-shaped electrodes remove tritium ions by either drifting them towards the walls where they are neutralized, or reflecting them back towards the source.

The beamline of the DPS-2F, between the WGTS and the CPS cryostat, is 7.3 m long. Each beam tube consists of a central tube, connected via bellows to a flange on each side. The central tubes have an inner diameter of 100 mm. The smallest diameter of the beamline is 85 mm, defined by the beamline instrumentation. The entire DPS2-F has a weight of about 10^4 kg and is fixed to the floor with earthquake protections. A computer-aided design (CAD) drawing of the DPS2-F is shown in Fig. 2.

2.1.2. Vacuum system

The required gas flow reduction factor is achieved by six TMPs (Leybold MAG-W 2800). Two TMPs are connected to PP0. The other four TMPs are located at the lower ends of PP1-4. Each TMP can be separated from the beamline by a DN 250 mm gate valve (VAT series 10). UHV vacuum gauges (MKS 421 inverted magnetron) are mounted on each pump port. The pressure along the DPS2-F beamline from PP0 to PP4 drops from approximately 10^{-6} mbar to 10^{-8} mbar. This absolute pressure reduction is not to be confused with the reduction of the tritium flow and the associated reduction of the partial pressure simulated here.

The superconducting magnets surrounding the beamline provide a guiding field of up to 5.5 T [11]. A passive magnetic shield encases each TMP to prevent eddy currents from heating, and possible crashing, of the fast-moving rotors [12].

2.2. The cryogenic pumping section

The last part of the transport and pumping section is the cryogenic pumping section (CPS), which has to reduce the residual gas flow by more than seven orders of magnitude. For this purpose, a cold argon frost layer prepared on the inner beamline surface, with an area of about 2 m^2 that is maintained at 3 K, adsorbs the incoming tritium molecules.

2.2.1. Geometry

In Fig. 3 a CAD drawing of the CPS is shown. The 12-ton CPS cryostat built by ASG Superconductors S.p.A. is about 6.5 m long and 4 m high. The beam tube elements of the CPS are subdivided into seven sections with a total length of roughly 7 m (inner diameter: ≥75 mm) and two pump ports. Each section is surrounded by a superconducting solenoid that produces the 5.6 T magnetic field [11] to guide β-electrons adiabatically through the CPS. The second and fourth beam tube are rotated by 15° from the longitudinal spectrometer axis, so that neutral tritium molecules would hit the beam tube wall, where they are adsorbed. Each beam tube is a stainless steel tube with gold plated on the inner surface. Additionally, there are 90 circular fins (length of 2 mm) inside each of the beam tube sections 2-4 enlarging the inner surface [6].

2.2.2. Vacuum system

The main part of the vacuum system of the CPS is the 3 m long cold trap (sections 2-5), covered by an argon frost layer at 3 K. The gold plated inner surface provides a clean surface for argon frost crystallization, as well as reducing the diffusion of hydrogen isotopes into the stainless steel. The cryogenic system includes two liquid helium (LHe) vessels; the first one at 4.5 K, the second one at 3 K. In order to reach 3 K in the second LHe vessel the 4.5 K helium is pumped down to a pressure of 0.16 bar and circulated through the cooling loop of the cold trap. For

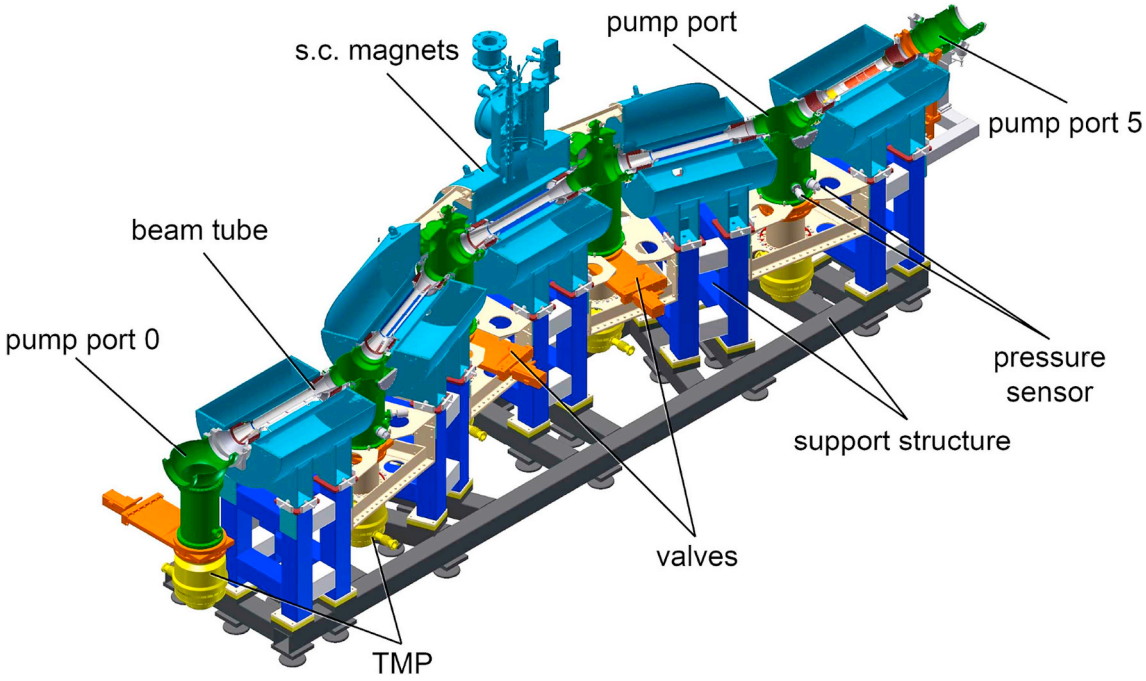

Fig. 2. Shown is the modular setup of the DPS2-F as a CAD drawing with a half-cut along the horizontal plane. Each beam tube (silver) is located in a warm bore of a superconducting solenoid (blue). The beam tubes are connected via the pump ports (green) to one beamline. The valves (orange) are located between the pump ports and the entrance of the TMPs (yellow). (For interpretation of the references to colour in this figure legend, the reader is referred to the Web version of this article.)

safety reasons the argon layer will be regenerated after 60 days of measurement time, which corresponds to an accumulated tritium activity below 1 Curie stored on the cold trap.

The other beam tube elements are cooled with liquid nitrogen and therefore operated at about 77 K. At PP1 and PP2 there are cold cathode gauges (MKS 421 inverted magnetron) to monitor the pressure in front of and behind the cold trap. TMPs are installed to both pump ports, but are turned off during standard KATRIN operation.

The tritium molecules adsorbed on the argon frost layer can re-desorb either via beta decay or by thermal desorption. Therefore, the pumping efficiency of the CPS cold section depends strongly on the temperature T. The mean sojourn time τ_{des} on the argon frost layer is [13].

$$\tau_{\mathrm{des}} = \tau_0 \cdot \exp\left(\frac{E_{\mathrm{des}}}{RT}\right), \tag{1}$$

where τ_0 is a material and gas specific time constant [14]. For the temperature range covered by the simulations in this paper, we used an approximate value of $\tau_0 = 10^{-13}$ s. E_{des} is the desorption energy for 1 mol of adsorbed gas, and $R = 8.314\,\mathrm{J\,mol\,K^{-1}}$ the molar gas constant.

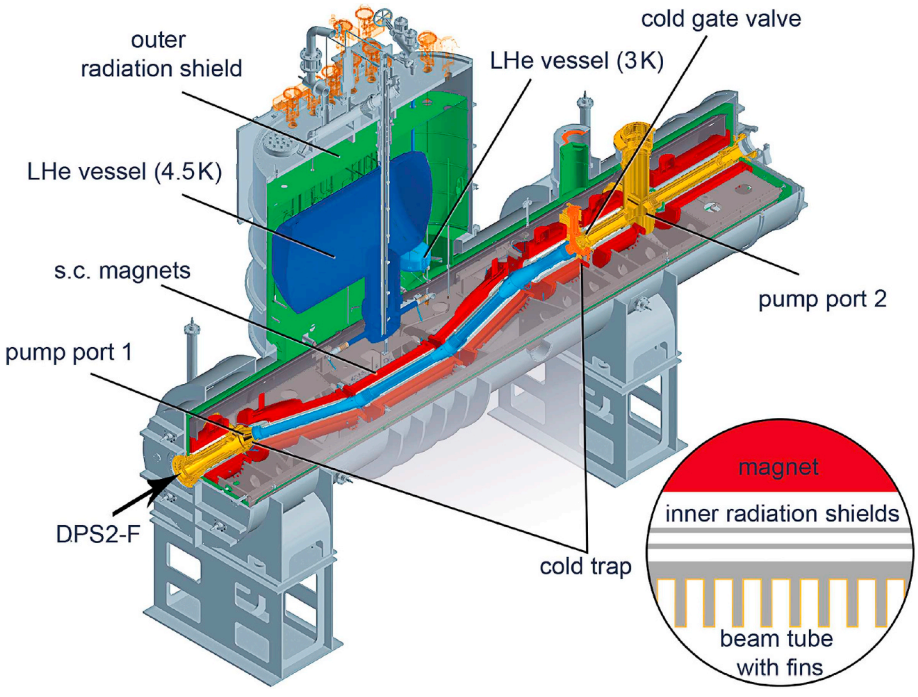

Fig. 3. CAD drawing of the CPS cryostat in 3/4 section. The gold-plated beam tube is surrounded by seven superconducting magnets (in red). The LHe vessel (4.5 K) provides a reservoir of 4.5 K cold helium, which is used for the cooling of the magnets and beam tube. The cold trap can be seen in blue between pump port 1 and the cold gate valve (CGV). The CGV is a safety valve operated inside the CPS at a temperature of 4.5 K. The differential pumping section (DPS2-F) is connected on the left side, the pre-spectrometer on the right side. (For interpretation of the references to colour in this figure legend, the reader is referred to the Web version of this article.)

2.2.3. Cold trap temperature

In each beam tube section of the cold trap the temperature is monitored by three rhodium-iron sensors with 50 mK accuracy. During the first activation of the 3 K-cooling system, the measured temperatures on the beam tube did not reach the expected 3 K [15], but varied between 3.4 K and 6.2 K.

In order to investigate the origin of the temperature discrepancy, the heat transfer module of the commercial simulation program COMSOL Multiphysics® was used with a finite-element-method simulation. A CAD model of the cold trap geometry is imported; the model includes the magnetic coils 2–5, the inner radiation shields, part of the 3 K-cooling loop connected to the beam tube, and the beam tube. The simulation is initialized with a fixed temperature of 4.5 K for the magnets and 3 K for the pipes of the cooling loops around the beamline. To reduce the calculation time, radiation is only allowed between opposite surfaces, e.g. between magnetic coils and inner radiation shield, while the radiation inside the beam tube is neglected. The heat load from elements, which are not explicitly simulated in the geometry model, is taken into account by assuming a uniform thermal black body radiation with a specific temperature. In COMSOL Multiphysics® this parameter is called ambient temperature. In order to minimize the differences between the simulated and the measured temperatures, the ambient temperatures for the different beam tube sections vary between 70 and 90 K. In this way the non-negligible radiation of the pump ports is included.

In Fig. 4, the deviations to the measurement results are shown. The errors correspond to the temperature gradient along the 30.0 mm × 14.8 mm × 19.5 mm copper sensor housing connected to the beamline. The largest discrepancies are located in the regions near to the beam tube bends and in beam tube section 5. The first one can be explained by the higher radiative heat loads on these regions due to the gaps between the inner radiation shields and the magnets. In beam tube section 5, a 180 mm stretch of the cooling loop is not brazed to the beam tube due to a repair in this area, which leads to a large area on the right side that has a temperature above 5 K. Regions near the cooling loop reach the expected 3 K while the temperature increases further away. Due to the narrower windings of the cooling loop towards the end of the beam tube sections, there are areas which are homogeneous at 3 K. Hot spots arise as a result of bolts connecting the warmer inner radiation shield to the beam tube sections 2-4. Except for these hot spots, most of the beamline areas, in particular those with the fins, are in a temperature range between 3 and 4 K. This simulated temperature profile is used in the next sections to calculate the reduction factor of the cold trap.

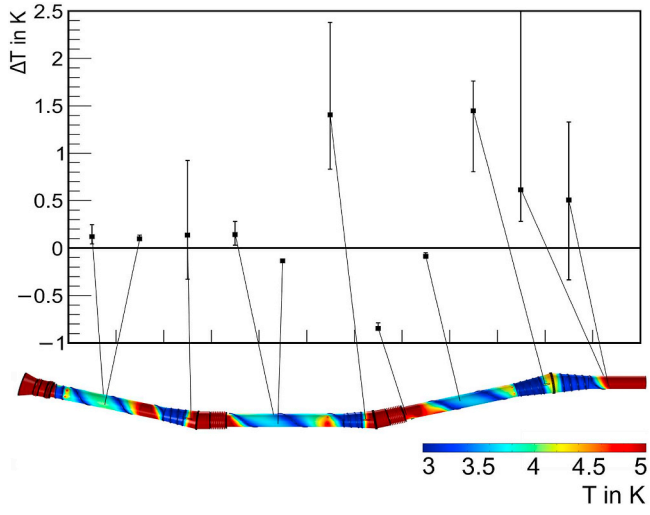

Fig. 4. Temperature deviation in Kelvin between measurement (T_{meas}) and simulation (T_{sim}). The error bars correspond to the simulated temperature variation across the connecting area of the sensor housing on the beam tube. At the bottom the simulated COMSOL Multiphysics® temperature profile is shown. The lines connect the $\Delta T = T_{meas} - T_{sim}$ points to the positions of the sensors.

3. The TPMC models

The TPMC models have been simulated with the software package MolFlow+ (version 2.5.6) [16]. The software is designed for particle tracking in the molecular flow regime. Its basic concepts are described in the following section.

3.1. Simulation with MolFlow+

MolFlow+ tracks test particles through the model of a vacuum chamber build up by a polygon mesh, of so-called facets. The particles only interact with the walls. When they hit a facet, they can either be adsorbed, reflected or transmitted. The properties of a facet are defined by various parameters, such as the temperature, the sticking factor defining the adsorption probability, the type of reflection, and the opacity. A facet can also be defined as a desorbing source of gas, where new particle tracks originate. Each track is simulated through a series of diffuse reflections and transmissions at facets until it is finally adsorbed. Each facet has three counters that are assigned for desorptions, hits and adsorptions; the counters are incremented accordingly when hit by a particle. A pump, such as a TMP, is represented by a circular facet the size of its entrance flange and a sticking factor $\alpha \in [0,1]$ equaling its pumping probability for the simulated gas type. If a particle is reflected, we assume diffuse reflection, following Knudsen's cosine law. The simulation of the new velocity of the scattered particle assumes total thermalization at the wall (accommodation coefficient = 1) with a Maxwell velocity distribution. Apart from the opaque facets representing the walls and internal structures of the vacuum chamber, the user can also define virtual facets, which are transparent. They do not affect the path of a particle, but count its transmission as a hit. A one-sided facet counts only particles impinging from one direction, while a two-sided one counts all particles. Virtual facets can be placed anywhere in the chamber, allowing us to monitor the pressure in the volume or to determine the transmission of particles from one part of the model to another.

After the simulation of an appropriate number of particle tracks, the results, represented by the three counters of each facet, are in general used to determine conductances, effective pumping speeds, and partial pressures. Details of the analysis methods for the DPS2-F and the CPS are described in the following sections.

3.2. The DPS2-F model

For DPS2-F particle tracking simulations, the MolFlow+ model shown in Fig. 5 is used [7]. It comprises about 19000 facets. The models of the WGTS [4] and the DPS2-F join at the entrance of PP0. The TMP sticking factors $\alpha = 0.252$ correspond to the pumping speed of TURBOVAC MAG W 2800 pumps for a gas mass of $m = 6\ \mathrm{g\ mol^{-1}}$, which has been chosen as the particle mass for the simulation of tritium molecules. It should be mentioned that the main systematic uncertainty of the simulations is the pumping probability α; the uncertainty is estimated using an empirical model for the pumping probability by Malyshev [10] to be 20%. The geometry of the electrodes of the ion detection and removal system inside the beam tube is included.

The particles desorb from the entrance facet of PP0 and are tracked through the complete geometry until they get pumped by one of the six TMPs or reach the entrance valve V2 towards the CPS. A sticking factor of $\alpha = 1.0$ has been assigned to the V2 facet. The entrance facet of PP0 is transparent. On the upstream side the geometry is terminated by the last beam tube element of DPS1-F, which ends in a facet with sticking factor $\alpha = 1.0$, representing the TMPs of the second stage of the DPS1-F.

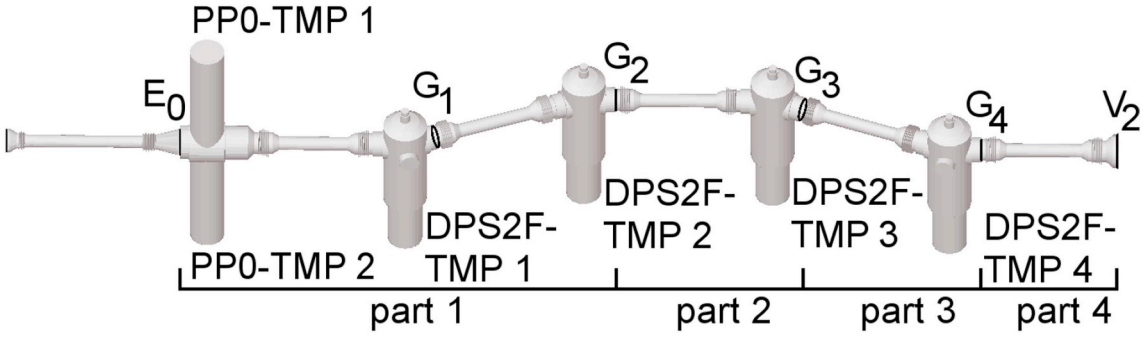

Fig. 5. The MolFlow+ model of the DPS2-F vacuum system. Some virtual facets, valves and the six active turbomolecular pumps are denoted. The four concatenated parts are indicated.

3.2.1. Concatenation of subsequent sections

The simulation of a flow reduction factor $R = \Phi_{in}/\Phi_{out}$ of 5 orders of magnitude and more is very time consuming. Therefore, the geometry of the DPS2-F was subdivided into four different parts (see Fig. 5). Each part was simulated independently, and the individual results were concatenated subsequently to derive the transmission probability, hits (for pressure) and adsorptions [7]. The reduction factor can be calculated by dividing the number of started particle tracks N_{des,E_0} at facet E_0 of PP0 by the number of particles N_{ads,V_2} adsorbed (leaving DPS2-F) at the gate valve V_2 between the DPS2-F and the CPS:

$$R_{tot} = R_1 \cdot R_2 \cdot R_3 \cdot R_4 = \left(\frac{N_{des,E_0}}{N_{hit,G_2}}\right)_{part\ 1} \cdot \left(\frac{N_{hit,G_2}}{N_{hit,G_3}}\right)_{part\ 2} \cdot \left(\frac{N_{hit,G_3}}{N_{hit,G_4}}\right)_{part\ 3} \cdot \left(\frac{N_{hit,G_4}}{N_{ads,V_2}}\right). \quad (2)$$

Here $N_{hit,G_{2-4}}$ are the number of particles passing the virtual facets in the downstream direction between the parts indicated in Fig. 5. Apart from the first part, the particle tracks were started at the entrances $G_{1\text{-}3}$ of the preceding beam tube section. Thus, the resulting solid-angle distribution of the velocities of the incoming tracks at facets $G_{2\text{-}4}$ was closer to the one expected for a single-pass simulation of the entire geometry. All simulations were done with the full model, changing only the desorbing facet where the tracks started. The simulations ran until the statistical uncertainty of the hits in the respective concatenating facets was better than 1%.

3.3. The CPS model

The MolFlow+ model of the CPS is shown in Fig. 6. It consists of about 58000 facets. The geometry of the CPS starts at valve V2 and ends at valve V4. Seven elements build up the complete beam tube. The TMPs at the two pump ports are turned off during standard operation, so the only pumping mechanism is cryosorption. For particles reflected back into the DPS2-F the last beam tube element is included up to the last DPS2-F pump port (PP4). Particles reaching this pump port are considered to be pumped out with high probability ($\alpha = 1$). This scheme ensures that the concatenation of the DPS2-F and CPS models is simulated with matching boundary conditions. A particle leaving the DPS2-F in the previous simulation through valve V2 is adsorbed ($\alpha = 1$), not taking into account that a fraction of the particles is actually reflected back into the DPS2-F. This is done in the subsequent CPS simulation, making sure that the back-reflection is not taken into account twice.

In order to reduce the computing time, the CPS model is subdivided into four parts, which are simulated separately and concatenated afterwards, similar to the DPS2-F (see Sec. 3.2.1). Since the sticking factor of the argon frost layer is not precisely known and also depends on the initial coverage, simulations were performed for $\alpha = 0.0$ to 0.7 in steps of 0.1. The upper value of 0.7 is the expected sticking factor for a well prepared argon layer at 3 K [17]. For facets not belonging to the cold trap, the sticking factor is set to $\alpha = 0.0$. At both ends of the model (DPS2F-PP4 and V4) it is set to $\alpha = 1$. In this case, the particles are either pumped out at DPS2F-PP4 or enter the pre-spectrometer volume, which has a diameter approximately twenty times larger than the CPS beam tube and a more than two orders of magnitude higher effective pumping speed for tritium than the conductance between the pre-spectrometer and the cold section of the CPS.

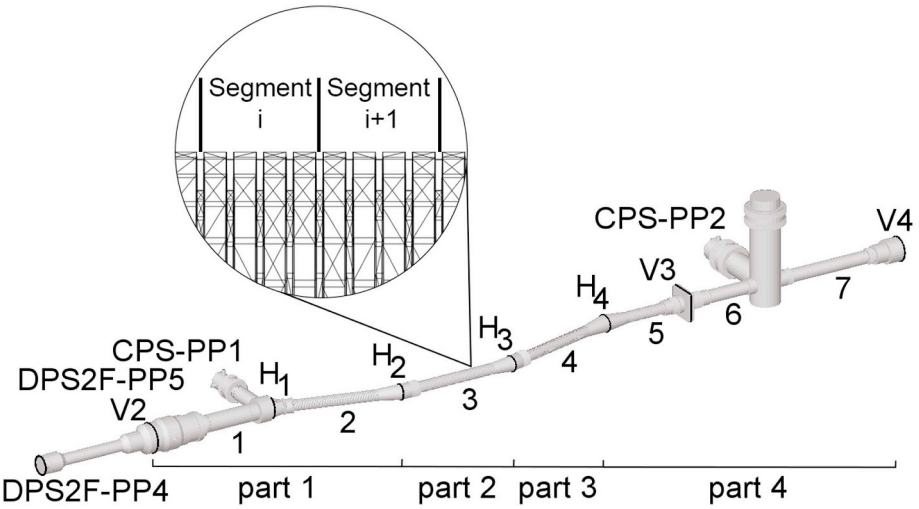

Fig. 6. The MolFlow+ model of the CPS vacuum system. Some virtual facets and real valves are marked by black lines. The four parts which are concatenated are marked.

The tracking of gas particles starts at valve V2. Before a particle reaches the cold trap it is only diffusely reflected when hitting a wall. Once a particle is adsorbed on a facet of the cold trap it sticks on it forever and the tracking path in MolFlow+ ends. According to Eq. (1) in Sec. 2.2.3 this model is not appropriate since particles can leave the facet by thermal desorption after some characteristic sojourn time τ_{des}. The redesorbed gas slowly migrates towards the end of the CPS, adding to the gas leaving through valve V4 towards the pre-spectrometer. Since the incoming gas flow from the DPS2-F is assumed to be constant, the reduction factor $R_{\mathrm{CPS}} = \Phi_{\mathrm{in}}/\Phi_{\mathrm{out}}$ of the CPS decreases over time.

Therefore a model has been developed, which combines the results from a multitude of MolFlow+ simulations and, in a second step, adds the effect of a finite sojourn time τ_{des} on the adsorbed tritium molecules. The basic idea is to subdivide the cold trap of the CPS beam tube into $n = 102$ smaller segments, and consider each segment as an individual cryo pump, where particles can adsorb and redesorb.

3.3.1. Segmentation of the cold trap

The number of adsorbed particles $A_i(t)$ sitting on the surface of segment i can either originate from the incoming gas flow Φ_{in} through the DPS-2F or from the desorption off other segments j. The change in the number of particles adsorbed on segment i can be described by a system of coupled differential equations

$$\frac{\mathrm{d}A_i(t)}{\mathrm{d}t} = \Phi_{\mathrm{in}} \cdot U^{\mathrm{ads},i}_{\mathrm{des,V2}} + \sum_{j=1}^{n} \left(\frac{A_j(t)}{\tau_{\mathrm{des}}} \cdot U^{\mathrm{ads},i}_{\mathrm{des},j} \right) - \frac{A_i(t)}{\tau_{\mathrm{des}}} \,. \tag{3}$$

The first term describes the adsorption rate on segment i from Φ_{in}. The parameter $U^{\mathrm{ads},i}_{\mathrm{des,V2}}$ is the adsorption probability on segment i for particles entering the CPS through valve V2. The second term is the sum of adsorptions on segment i of particles originating from desorptions off segments j of the cold trap with a rate $A_j(t)/\tau_{\mathrm{des}}$. Similar to the first term $U^{\mathrm{ads},i}_{\mathrm{des},j}$ describes the probability that a particle desorbed at segment j is adsorbed on segment i. The third term subtracts the rate of desorbing particles from segment i. All adsorption probabilities can be combined in a matrix U determined by MolFlow+ simulations.

The segments in the cylindrical part of the beam tubes were chosen to be 3.2 cm long, which corresponds to the distance between four consecutive fins (see Fig. 6). The cones at the ends of each beam tube element were simulated as longer segments. In addition, four simulations were necessary for simulating the gas inlet at valve V2, and the concatenations of the four parts, similar to the DPS2-F, for calculating the direct transmission through the CPS from V2 to V4. For the direct gas flow through V2, the results from these concatenating simulations were also used to calculate the adsorption probabilities $U^{\mathrm{ads},i}_{\mathrm{des,V2}}$ for segments beyond H2 (see Fig. 6). For each segment i the counters of the corresponding facets were added up to the number of desorptions $N_{\mathrm{des},i}$, adsorptions $N_{\mathrm{ads},i}$ and hits $N_{\mathrm{hit},i}$. With these numbers the probability matrices for desorptions (U) and pressure (hit matrix V) can be calculated:

- $U^{\mathrm{ads},i}_{\mathrm{des},j} = \frac{N_{\mathrm{ads},i}}{N_{\mathrm{des},j}}$ is the probability that a particle desorbing from segment j is adsorbed on segment i.
- $V^{\mathrm{hit},i}_{\mathrm{des},j} = \frac{N_{\mathrm{hit},i}}{N_{\mathrm{des},j}}$ is the probability that a particle desorbing from segment j hits segment i.

It is $j \in [0,102]$ and $i \in [1,103]$ for $U^{\mathrm{ads},i}_{\mathrm{des},j}$ where $j = 0$ represents the inlet valve V2, $i, j \in [1,102]$ represent the 102 segments, and $i = 103$ the exit valve V4. For $V^{\mathrm{hit},i}_{\mathrm{des},j}$ it is $j \in [0,102]$ and $i \in [1,105]$. The indices $i = 104$ and $i = 105$ represent the facets where the pressure gauges are located in CPS-PP1 and CPS-PP2, respectively.

In order to attain better statistics in the region, where most of the gas is adsorbed, the concatenations of the CPS geometry were also applied for calculating the hit $V^{\mathrm{hit},j}_{\mathrm{des},i}$ and adsorption $U^{\mathrm{des},j}_{\mathrm{ads},i}$ probabilities for desorptions from the segments of the first cold trap section ($j \in [1,27]$):

i) If the segments i and j lie in the same or in the neighboring beam tube section it is:

$$U^{\mathrm{ads},i}_{\mathrm{des},j} = \frac{N_{\mathrm{ads},i}}{N_{\mathrm{des},j}} \text{ and } V^{\mathrm{hit},i}_{\mathrm{des},j} = \frac{N_{\mathrm{hit},i}}{N_{\mathrm{des},j}}.$$

ii) If the segments i and j are separated by exactly one beam tube section with the ending facet H_3 it is:

$$U^{\mathrm{ads},i}_{\mathrm{des},j} = \frac{N_{\mathrm{hit,H_3}}}{N_{\mathrm{des},j}} \cdot \left(\frac{N_{\mathrm{ads},i}}{N_{\mathrm{hit,H_3}}} \right)_{\mathrm{part\ 3}} \text{ and}$$

$$V^{\mathrm{hit},i}_{\mathrm{des},j} = \frac{N_{\mathrm{hit,H_3}}}{N_{\mathrm{des},j}} \cdot \left(\frac{N_{\mathrm{hit},i}}{N_{\mathrm{hit,H_3}}} \right)_{\mathrm{part\ 3}} .$$

iii) If the segments i and j are separated by exactly two beam tube sections with the ending facets H_3 and H_4 it is:

$$U^{\mathrm{ads},i}_{\mathrm{des},j} = \frac{N_{\mathrm{hit,H_3}}}{N_{\mathrm{des},j}} \cdot \left(\frac{N_{\mathrm{hit,H_4}}}{N_{\mathrm{hit,H_3}}} \right)_{\mathrm{part\ 3}} \cdot \left(\frac{N_{\mathrm{ads},i}}{N_{\mathrm{hit,H_4}}} \right)_{\mathrm{part\ 4}} \text{ and}$$

$$V^{\mathrm{hit},i}_{\mathrm{des},j} = \frac{N_{\mathrm{hit,H_3}}}{N_{\mathrm{des},j}} \cdot \left(\frac{N_{\mathrm{hit,H_4}}}{N_{\mathrm{hit,H_3}}} \right)_{\mathrm{part\ 3}} \cdot \left(\frac{N_{\mathrm{hit},i}}{N_{\mathrm{hit,H_4}}} \right)_{\mathrm{part\ 4}} .$$

This case-by-case analysis was constructed in such a way that the solid angle under which a particle enters the next part of the CPS is comparable to a single-pass simulation. For elements $j \in [28,102]$, the concatenation has not been applied since the first test simulations indicated a coverage reduced by several orders of magnitude compared to the first CPS simulation part.

3.3.2. Time-dependent gas flow

In order to describe time-dependent processes the coupled differential equations (3) of the amounts of adsorbed gas on each segment are numerically integrated over time with discrete steps of Δt. An analytical solution of Eq. (3) was not pursued due to the high number ($>10^4$) of independent coefficients $U^{\mathrm{ads},i}_{\mathrm{des},j}$ which leads to a complex determination of eigenvalues and eigenvectors. The gas inlet into the CPS starts at $t_0 = 0$ s. The inlet rate Φ_{in} from the DPS2-F stays constant over the whole time. In the simulation, this gas inlet is represented by the desorption of particles from facet V2. The time difference between t_0 and any other time t_n is subdivided into n intervals with length Δt. At the time $t_0 = 0$ s, it is assumed that there are no particles in the system at all ($A_i(0) = 0$), which defines the boundary conditions for the numerical integration. After the first iteration at $t_1 = \Delta t$ the amount of gas adsorbed on a specific segment i, is described by

$$A_i(t_1) = \Phi_{\mathrm{in}} \cdot \Delta t \cdot U^{\mathrm{ads},i}_{\mathrm{des,V2}} \,. \tag{4}$$

For any time $t_n = n \cdot \Delta t > t_1$ the number of adsorbed particles on segment i is defined as

$$\begin{aligned} A_i(t_n) &= A_i(t_{n-1}) + \Phi_{\mathrm{in}} \cdot \Delta t \cdot U^{\mathrm{ads},i}_{\mathrm{des,V2}} \\ &\quad + \textstyle\sum_{j=1}^{102} \left(A_j(t_{n-1}) \frac{\Delta t}{\tau_{\mathrm{des}}} U^{\mathrm{ads},i}_{\mathrm{des},j} \right) - A_i(t_{n-1}) \frac{\Delta t}{\tau_{\mathrm{des}}} \end{aligned} \tag{5}$$

for $i \in [1,102]$.

The first term represents the number of adsorbed particles at the time t_{n-1}. The second term takes the gas inlet between t_{n-1} and t_n into account. The factor $A_j(t_{n-1})\Delta t/\tau_{\mathrm{des}}$ in the third term equals the amount of desorbed gas from segment j. By multiplying this with $U^{\mathrm{ads},i}_{\mathrm{des},j}$, one gets the number of particles desorbed from segment j and adsorbed on

segment i during the time interval Δt. For the gas Φ_{out} leaving the CPS towards the spectrometer section through valve V4 ($i = 103$), we neglect any gas coming back to the CPS due to the large pumping speed of the pre-spectrometer. With

$$\begin{aligned}\Phi_{out} &= \frac{A_{103}(t_n) - A_{103}(t_{n-1})}{\Delta t} \\ &= \Phi_{in} \cdot U^{ads,103}_{des,V2} + \sum_{j=1}^{102} \left(\frac{A_j(t_{n-1})}{\tau_{des}} U^{ads,103}_{des,j} \right),\end{aligned} \tag{6}$$

we can describe the time-dependent flow reduction as

$$R(t_n) = \frac{\Phi_{in}}{\Phi_{out}} = \frac{\Phi_{in}}{\Phi_{in} \cdot U^{ads,103}_{des,V2} + \sum_{j=1}^{102} \left(\frac{A_j(t_{n-1})}{\tau_{des}} U^{ads,103}_{des,j} \right)} \tag{7}$$

The pressure at segment i in the TPMC simulation can be determined from the number of hits $N_{hit,i}$, the area of the segment F_i, the mean thermal velocity $\bar{c}$, the number of desorbed particles $N_{des,j}$ from segment j, and the actual gas flow (or outgassing rate) into the chamber $Q_j(t)$ [18]:

$$p_{ij}(t) = \frac{4}{\bar{c}} \frac{Q_j(t)}{F_i} \frac{N_{hit,i}}{N_{des,j}} = \frac{4}{\bar{c}} \frac{Q_j(t)}{F_i} \cdot V^{hit,i}_{des,j} \,. \tag{8}$$

Multiplying the particle flow Φ_{in} with the Boltzmann constant k_B and the temperature T, the pressure after the first iteration at $t_1 = \Delta t$ is

$$p_i(t_1) = \frac{4}{\bar{c}} \frac{\Phi_{in} \cdot k_B T}{F_i} \cdot V^{hit,i}_{des,V2} \,, \tag{9}$$

and for $t_n = n \cdot \Delta t$:

$$\begin{aligned}p_i(t_n) &= p_i(t_1) + \sum_{j=1}^{102} p_{ij} \\ &= p_i(t_1) + \sum_{j=1}^{102} \left(\frac{4}{\bar{c}} \frac{A_j(t_{n-1}) \cdot k_B T}{F_i \cdot \tau_{des}} V^{hit,i}_{des,j} \right) \\ &= \frac{4 \cdot k_B T}{\bar{c} \cdot F_i} \left(\Phi_{in} \cdot V^{hit,i}_{des,V2} + \sum_{j=1}^{102} \left(\frac{A_j(t_{n-1})}{\tau_{des}} V^{hit,i}_{des,j} \right) \right).\end{aligned} \tag{10}$$

The pressures at CPS-PP1 and CPS-PP2 are particularly relevant since these are measurable quantities. From simulations, the pressure ratio is

$$\frac{p_{PP1}(t_n)}{p_{PP2}(t_n)} = \frac{\frac{\Phi_{in}}{F_{PP1}} \cdot V^{hit,PP1}_{des,V2} + \sum_{j=1}^{102} \frac{A_j(t_{n-1})}{\tau_{des}} \frac{1}{F_{PP1}} V^{hit,PP1}_{des,j}}{\frac{\Phi_{in}}{F_{PP2}} \cdot V^{hit,PP2}_{des,V2} + \sum_{j=1}^{102} \frac{A_j(t_{n-1})}{\tau_{des}} \frac{1}{F_{PP2}} V^{hit,PP2}_{des,j}} \,. \tag{11}$$

This ratio is correlated with the flow reduction:

$$R(t_n) = k(t_n) \cdot \frac{p_{PP1}(t_n)}{p_{PP2}(t_n)} \,. \tag{12}$$

By simulating both the flow reduction and the pressure ratio, the ad hoc factor $k(t_n)$ can thus be determined. This result is essential for interpreting measured pressure values at the pump ports.

3.3.3. Including the beamline temperature profile

The COMSOL Multiphysics® simulation of the CPS cold trap temperature profile in Sec. 2.2.3 revealed inhomogeneities of several Kelvin. These inhomogeneities have a non-negligible influence on the pumping efficiency of the cold trap; in particular, the mean sojourn time τ_{des} is affected. This can be included in the analysis of the MolFlow + simulations by calculating the weighted mean of all $\bar{\tau}_{des}$ in the system:

$$\begin{aligned}\bar{\tau}_{des} &= \frac{\sum_{i=1}^{n} \tau_0 \cdot \exp\left(\frac{E_{des}}{RT_i}\right) A_i}{\sum_{i=1}^{n} A_i} \\ &= \begin{cases} 5.4 \times 10^{6}\text{s} & \text{for} \quad 1200\ \text{J mol}^{-1} \\ 1.5 \times 10^{10}\text{s} & \text{for} \quad 1400\ \text{J mol}^{-1} \\ 4.1 \times 10^{13}\text{s} & \text{for} \quad 1600\ \text{J mol}^{-1} \end{cases}.\end{aligned} \tag{13}$$

The weight A_i is the area of one of the corresponding beamline surface elements with temperature T_i of the COMSOL Multiphysics® mesh. With a fixed desorption energy E_{des}, the flow reduction can now be calculated on an absolute time scale. Since the magnitude of the desorption energy E_{des} is not known, a range from 1200 J mol^{-1} to 1600 J mol^{-1} is investigated. The lower boundary is taken from the estimation given in Ref. [19], the upper boundary can be estimated from the first retention measurements which will not be discussed in detail within this publication.

3.3.4. Tritium decay

For radioactive adsorbates, the sojourn time can no longer be described solely by the desorption time τ_{des} given in Eq. (1). One has to take the influence of radioactive decays inside of the adsorbens into account. In addition to the released decay products, a tritium decay can also induce the desorption of other atoms in its vicinity, including both tritium and argon. The amount of desorbed tritium $\eta(s)$ from a single β-decay inside the argon frost layer depends on the surface coverage s. It can be described with the following formula investigated by Malyshev [20]:

$$\eta(s) = \eta_{max} \cdot \frac{s}{s + s_m} \,, \tag{14}$$

where η_{max} denotes the upper limit for the desorption yield, and s_m the kink between the linear rise and the plateau where $\eta(s)$ reaches saturation. The values of these parameters are estimated with $\eta_{max} = 10^3$ T_2/delay and $s_m \approx 4 \times 10^{14}$ T_2 cm^{-2} [20]. Given this relation, the effective desorption time can be derived from the differential equation

$$\frac{dN}{dt} = -N \cdot \left(\frac{1}{\tau_{des}} + \sigma \cdot \eta(s) \cdot \lambda_T \right), \tag{15}$$

describing the rate of desorbing particles by both thermal desorption and radioactive desorption. The latter is described by the decay constant λ_T. The variable σ is used to describe the gas composition and can take values from 0 to 2 depending on the amount of tritium atoms of the adsorbed isotopologues (H_2: $\sigma = 0$, HT: $\sigma = 1$, T_2: $\sigma = 2$, …). The probability density distribution $\rho(t)$ for the sticking time is then given by

$$\rho(t) = \frac{1}{\tau_{eff}} \cdot \exp\left(-\frac{t}{\tau_{eff}} \right) \tag{16}$$

with the effective time constant

$$\tau_{eff} = \left(\frac{1}{\tau_{des}} + \sigma \cdot \eta(s) \cdot \lambda_T \right)^{-1} \,. \tag{17}$$

With the additional decay-induced desorptions, the effective sojourn time will no longer increase with falling temperatures but converges towards a limit as is shown in Fig. 7.

4. Semi-Analytical Tracking Model of the CPS

Since tritium decay plays a major role in decreasing the sojourn time of a tritiated molecule inside the cold pump, this effect needs to be taken into account when simulating the tritium reduction factor of the CPS. The currently available simulation programs for TPMC do not meet the requirements of simulating large reduction factors in combination with radioactive adsorbates and strongly inhomogeneous temperature profiles. This was the reason for developing a custom C++-based Semi-Analytical Tracking Model. By disassembling the geometry given in Fig. 6 into its basic geometric primitives (namely cylinders, cones and cuboids), the motion and interaction points with the surface can be calculated analytically. For the desorption process, a multistage Monte Carlo sampling is needed to determine both the sojourn time and the direction in which a particle desorbs. The former is done by sampling from the distribution given in Eq. (16), the latter with a cosine law sampling [21]. The advantage of the semi-analytical tracking is that the model offers the possibility to integrate three-

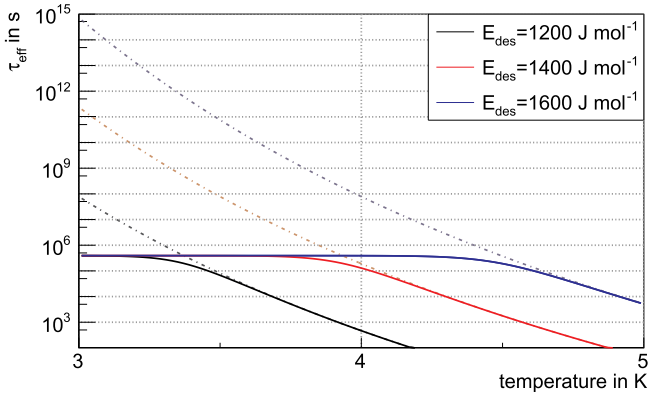

Fig. 7. Course of the effective desorption time for different desorption energies at a surface coverage of $s = 10^{15}\,T_2cm^{-2}$ ($\sigma = 2$) compared to the case without radioactivity (dashed lines).

dimensional models not only for the temperature, but also for the surface coverage along the beamline, which will be discussed in more detail in Sec. 5.2.2. The integration of a temperature profile will provide a more precise simulation result than just assuming an average beam tube temperature, since there are regions that are more likely to be hit because of the rotation of the beam tube sections. Therefore a very detailed temperature model from the simulations in Sec. 2.2.3 with more than 12 000 equally distributed temperatures along beam tube sections 2 to 5 of the CPS is used for the simulations. Compared to the TPMC simulations in Sec. 3.3, the Semi-Analytical Tracking Model requires a new simulation for each desorption energy by changing τ_{des} and cannot be computed from one set of simulations.

4.1. Reduction factor calculation

With the Semi-Analytical Tracking Model, the migration time of a single particle along the entire CPS is calculated. The simulation of a particle track can have four different outcomes:

i) The particle leaves the CPS through valve V4 into the pre-spectrometer. Only these events contribute to the determination of the reduction factor.
ii) The particle is reflected back into the DPS2-F, where it reaches PP4 and is pumped out by the TMP.
iii) The simulation is aborted because the particle takes longer to leave the CPS than the initially set maximal migration time.
iv) The particle decays while still in the CPS, most likely being adsorbed on the argon frost layer.

Only 1% of the tritium decays during the nominal operation time of 60 days between subsequent regenerations of the argon frost layer, which is why the loss of tritium due to its decay is neglected in this simulation. The results can also be used for stable isotopes, such as hydrogen or deuterium, if the mean sojourn time τ_{des} is much longer than the time of flight between two hits of the walls.

To extract the reduction factor of the cold trap, a significant amount of particle tracks and the corresponding migration times need to be calculated. Storing the information into a histogram, normalized to the total number of simulated particle tracks, gives a probability density distribution $m(t)$ for the time t which a molecule needs to migrate along the geometry. Since $m(t)$ depends on the desorption energy, tritium purity, sticking probability, and the temperature, these simulations have to be repeated for each parameter setting. Once the probability density has been simulated, it can be transformed into a time-dependent tritium flux $\Phi_{out}(t)$ from the downstream end of the CPS to the pre-spectrometer. This is done by integrating over the migration probability $m(t)$ and multiplying with the expected constant tritium flux $\Phi_{in} = 10^{12}$ molecules s^{-1} [7] from the DPS2-F into the CPS

$$\Phi_{out}(t) = \Phi_{in} \int_0^t m(t')\,dt'. \tag{18}$$

The reduction factor $R(t)$ after time t of continuous operation is defined as the ratio of the outgoing and incoming flux:

$$R(t) = \frac{\Phi_{in}}{\Phi_{out}(t)} = \left(\int_0^t m(t')\,dt'\right)^{-1}. \tag{19}$$

The transmission probability density and its integral (Eq. (18)) are shown in Fig. 8. Although the distributions were simulated with up to 2.5×10^{11} events each, the simulations provide virtually no events in the region between 0 and 60 days for reduction factors $R(60\,d) > 10^{12}$. In this case a linear interpolation between the first non zero bin and the origin (where the tritium flow is expected to be zero) is applied.

5. Results

In the following, the simulation results of the flow reduction of both DPS2-F and CPS are presented. In Secs. 3 and 4, two different approaches were introduced. The DPS2-F results are solely based on MolFlow+ simulations, while the CPS results were complemented by the Semi-Analytical Tracking Model.

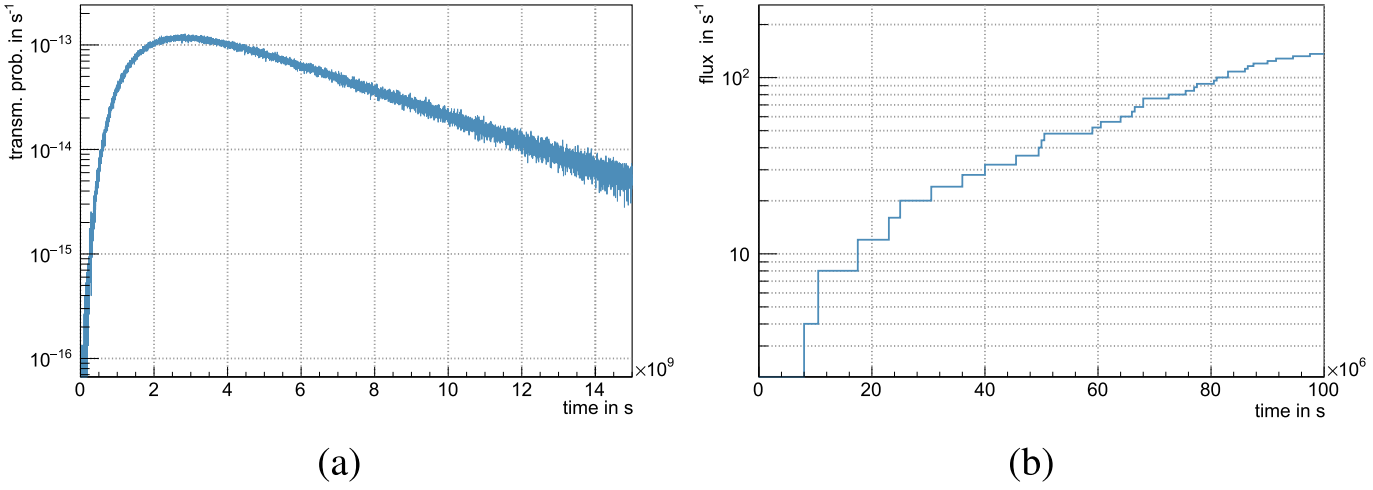

Fig. 8. (a) Transmission probability function for a desorption energy of 1200 J mol^{-1} with pure tritium ($\sigma = 2$); (b) zoom to the region of interest of the resulting tritium flux into the pre-spectrometer according to Eq. (18).

Table 1
Results of the four parts of the DPS2-F gas flow simulation with MolFlow+.

Part	Desorption	Inlet & outlet	Inlet counts	Outlet counts
1	E_0	E_0 & G_2	36901582	466310
2	G_1	G_2 & G_3	3385527	342948
3	G_2	G_3 & G_4	809346	82173
4	G_3	G_4 & V_2	2142160	104502

5.1. DPS2-F

The DPS2-F simulation has been split into four parts as described in Sec. 3.2. Table 1 gives an overview of the results.

Concatenating all four simulations to an overall reduction factor yields

$$R_{\mathrm{DPS2-F}} = (1.577 \pm 0.008_{\mathrm{stat.}}) \times 10^5 \tag{20}$$

with the statistical uncertainty calculated by using binomial statistics. To estimate the systematic uncertainty of the TMP pumping probability (see Sec. 3.2) a dedicated simulation with $\alpha = 0.202$ was performed. The result

$$R^{\mathrm{lower}}_{\mathrm{DPS2-F}} = (8.99 \pm 0.05_{\mathrm{stat.}}) \times 10^4 \tag{21}$$

gives a lower limit for the reduction factor with a 20% reduction of pumping probability.

5.2. CPS

5.2.1. MolFlow+

Two different scenarios were simulated with MolFlow+. The first one is the standard neutrino mass measurement; the parameter of interest is the reduction factor. The other scenario is the commissioning measurement with D_2; the parameters of interest are the pressures at both pump ports. In the commissioning simulation, the inlet valve V2 and the outlet valve V4 are assumed to be closed, while they are opened during the neutrino mass measurement simulation.

Combining the resulting values $R(t)$ for the neutrino mass measurement simulation with $p_{\mathrm{PP1}}(t)$ and $p_{\mathrm{PP2}}(t)$ for the commissioning measurement simulation, the factor $k(t)$ of Eq. (12) was determined.

The simulation results for the two relevant parameters are displayed in Fig. 9(a) and (b). Since the mean sojourn time τ_{des} is unknown, the time axes are normalized to τ_{des}. The time interval for the iterative integration was set to $\Delta t = 0.01 \cdot \tau_{\mathrm{des}}$. As expected, the reduction factor and the pressure ratio show a similar time-dependent behavior. Over a period of $2\tau_{\mathrm{des}}$ both parameters decrease by 2–3 orders of magnitude, except for $\alpha = 0.0$ where they stay constant as there is no cryosorption at all. Lower sticking coefficients result in lower reduction factors and pressure ratios. The results for the ad hoc factor $k(t)$ are important for interpreting the D_2 commissioning measurements. The simulated values lie between 8.5 and 21.5, and stay more or less constant.

For the nominal KATRIN operation sufficient tritium suppression for the whole 60-day run period is of paramount importance. To understand the long-term suppression, the x-axis in Fig. 9(a) has to be multiplied with a constant τ_{des}. Therefore, the desorption energy E_{des} is fixed, and the inhomogeneous beamline temperature profile is included according to Sec. 3.3.3. This has been done for $\alpha = 0.7$ and three different desorption energies $E_{\mathrm{des}} = 1200$ J mol^{-1}, 1400 J mol^{-1}, and 1600 J mol^{-1}. The results are shown in Fig. 10.

5.2.2. Semi-Analytical Tracking Model

Because of the dependence of τ_{eff} on $\eta(s)$, a detailed knowledge of the surface coverage s along the segments of the CPS is required to simulate the impact of radioactive decays on the tritium reduction factor. With the cold trap temperature profile implemented in the simulation code, the surface coverage turns from a smooth distribution into the density map shown in Fig. 11. The correlation between the lower temperatures and a high surface coverage can be easily explained by the mean sojourn time of the molecules adsorbed on the argon frost, which depends strongly on the local temperature (see Eq. (16)). The inhomogeneous temperature profile leads to an enhanced migration from regions of higher temperatures to regions of lower temperatures. As shown in Fig. 12, the mean surface coverage

$$\bar{s} = \frac{\sum_i s_i \cdot n_i}{n_{\mathrm{tot}}} \tag{22}$$

decreases almost exponentially from about 10^{15} T_2 cm^{-2} at the upstream entrance to 10^9 T_2 cm^{-2} or less at the downstream end of the CPS. Here s_i denotes the surface coverage of bin i in Fig. 11 and n_i the corresponding amount of molecules. Calculating the average weighted by particles within a given bin instead of its area is required to correctly simulate β-desorptions as described in Sec. 3.3.4.

To cover the expected range of the desorption energy (see Sec. 3.3.3), a set of simulations reaching from $E_{\mathrm{des}} = 1200$ J mol^{-1} to $E_{\mathrm{des}} = 1600$ J mol^{-1} has been performed. For non-radioactive gases with desorption energies above 1200 J mol^{-1}, this simulation method is not suitable since the probability function used to calculate the reduction (see Eq. (19)) has no entries close to the region from $t = 0$ days to $t = 60$ days. Therefore the uncertainty of any extrapolation would span several orders of magnitude.

But as soon as radioactive desorption is considered, the sojourn time and the reduction factor are drastically reduced. In this case, the Semi-Analytical Tracking Model is valid even for higher desorption energies and lower temperatures where τ_{eff} converges towards a constant value, as shown in Fig. 7. This can be seen in Fig. 13 where the tritium reduction factor rises slower with larger desorption energies for T_2 than it does for isotopologues with only one tritium atom (HT, DT).

In order to reduce the complexity of the simulation code, a static mean surface coverage $\bar{s}$ after 60 days of each beam tube section is used. These values were obtained from preceding simulations for each binding energy without taking radioactive desorptions into account (see Fig. 12). Using $\bar{s}$ is justified, since the influence of radioactive decays is only significant in regions with low temperature (see Fig. 7), where the majority of the molecules is adsorbed. Because no time dependency is implemented, the results for the reduction factor have to be seen as a conservative lower limit. Here the influence of the desorption energy on the reduction factor is only in the range of two orders of magnitude. Even for the very conservative assumption of a static surface coverage and a desorption energy of 1200 J mol^{-1}, the simulation yields a reduction factor of at least 2.6×10^{10}, which exceeds the requirements by three orders of magnitude. The simulation results for higher binding energies are given in Table 2.

6. Discussion

With the specified reduction factor of 10^5 for the DPS2-F, the results obtained with the MolFlow+ simulations are right on target. The lower limit for the reduction factor takes into account the conservative uncertainty of the TMP pumping probabilities for T_2.

On the other hand, the MolFlow+ results for the CPS show a reduction factor that exceeds the specified goal of 10^7 by several orders of magnitude. For the safe operation of KATRIN, it is important to understand the accuracy of these results.

The impact of the cold trap capacity on the sticking probability has not been included in the model. After 60 days of KATRIN operation, approximately 1.7% of the total cold trap capacity is reached [7]. Further, it is assumed that the first 1.7% of the trap is covered to 100% ($\alpha = 0$), while the rest is free of adsorbates. Under the assumption, the reduction factor drops exponentially along the cold trap; the final value of 2.7×10^{11} (see Fig. 10) for the lower limit of E_{des} would be reduced by 36%.

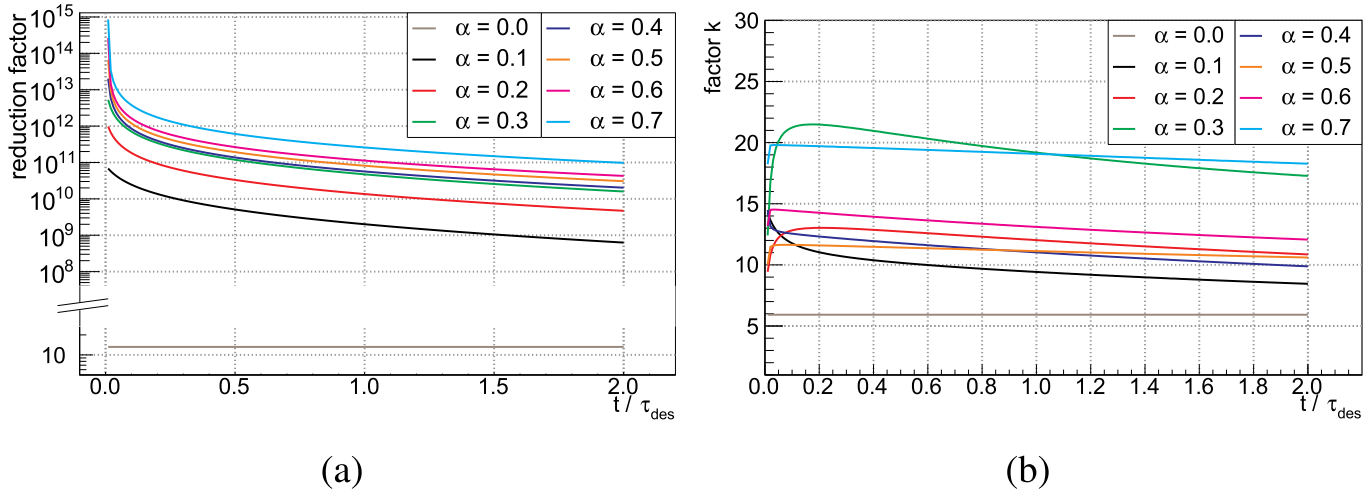

Fig. 9. CPS parameters for different sticking coefficients of the argon frost layer from $\alpha_{AR} = 0.0$ to 0.7, simulated with MolFlow+. The reduction factors for standard tritium operation (a) and the factor $k = R/(p_{PP1}/p_{PP2})$ (b) are shown. The pressure ratios p_{PP1}/p_{PP2} of pump port 1 to pump port 2 have been simulated for the D_2 commissioning measurement scenario. For $\alpha_{Ar} = 0.0$, the constant values are $R \approx 13.2$ and $k \approx 5.9$.

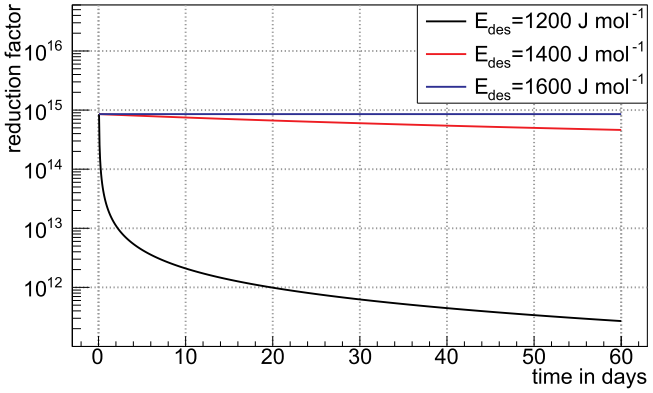

Fig. 10. The reduction factor for three different desorption energies E_{des} and $\alpha = 0.7$ with the inhomogeneous CPS beam tube temperature profile, simulated with MolFlow+. The effect of tritium migration can be clearly seen for the lower desorption energies.

A second source of systematic uncertainties is the concatenation algorithm of the four independently simulated parts of the CPS MolFlow + geometry. By comparing simulations with a small sticking coefficient $\alpha = 0.1$ for a single-pass simulation and with concatenation, the total error is estimated to be less than a factor of two.

The analysis of the time dependence with MolFlow+ simulations provides results for a time scale normalized to the sojourn time τ_{des}. In order to extract results on an absolute time scale, an appropriate range for the unknown desorption energy E_{des} has to be estimated. Reasonable values lie between 1200 J mol^{-1} and 1600 J mol^{-1}. In addition the temperature inhomogeneity of the cold trap was included by calculating an effective mean sojourn time $\bar{\tau}_{des}$ (see Sec. 3.3.3). This is justified by the large number of adsorptions on different segments when particles migrate through the cold trap.

Considering all of the relevant systematic uncertainties, the results' accuracy is assumed to be on the order-of-magnitude level. The simulations are very important for characterization measurements of the CPS cold trap with D_2 because the reduction factor cannot be measured directly. The measurements might also help to reduce the large uncertainties of the input parameters. For the standard KATRIN operation, additional β-induced desorptions from tritium decays have to be taken into account, which would reduce the assumed sojourn time even further. Despite all these uncertainties in the MolFlow+ simulations, the expected reduction factor still exceeds the nominal value by several orders of magnitude.

Compared to the D_2 simulations with MolFlow+, the Semi-Analytical Tracking Model for tritiated isotopologues has a significantly lower reduction factor, as shown in Fig. 13. The reduction factor for tritium still exceeds the requirements by far. A necessary simplification had to be made in order to attain the reduction factor for radioactive adsorbates. This simplification includes the assumption of a time independent, mean surface coverage per beam tube section, as described in Sec. 5.2.2. This approach overestimates the surface coverage and results in a conservative limit.

Another systematic uncertainty arises from the linear interpolation of the cumulative probability density function of the migration time (see Fig. 8) for $t < 60$ days. If no event is produced in this region, a conservative lower limit of 2.5×10^{11} for the reduction factor can be inferred.

In Fig. 14, the results of both simulation methods are compared for D_2 simulations for an assumed desorption energy of 1200 J mol^{-1}. The two very different approaches show similar results. After 60 days, the results $R = 2.7 \times 10^{11}$ for MolFlow+ and $R = 4.0 \times 10^{11}$ for the Semi-Analytical Tracking Model agree to within a factor of two. Taking into account the complexity and different approximations of both methods, the results can still be considered to be in good agreement.

7. Conclusions

In the KATRIN experiment, it is mandatory to reduce the tritium gas flow between the WGTS and the pre-spectrometer by at least 14 orders of magnitude. Tritium decays inside the spectrometer section would otherwise increase the background rate of the experiment, limiting the ultimate sensitivity for the neutrino mass. For this reason, the differential pumping sections DPS1-F ($R_{DPS1\text{-}F} = 2 \times 10^3$ simulated in Ref. [4]), DPS2-F, and the cryogenic pumping section CPS are located between the WGTS and the spectrometer section to reduce the tritium flow accordingly.

While the simulated reduction factor ($R_{DPS2\text{-}F} > 9 \times 10^4$) of the TMP-based DPS2-F was close to the initial design value of 10^5, the simulation of the CPS proved to be more challenging. Two different models were used for the simulation of the CPS in the molecular flow regime: a TPMC simulation with MolFlow+ and a Semi-Analytical Tracking Model developed in C++. Both models are in good agreement with each other. The inhomogeneities of the temperature profile of the CPS cold trap, used by both models, were simulated with COMSOL Multiphysics®. The wide range of possible input parameters for the

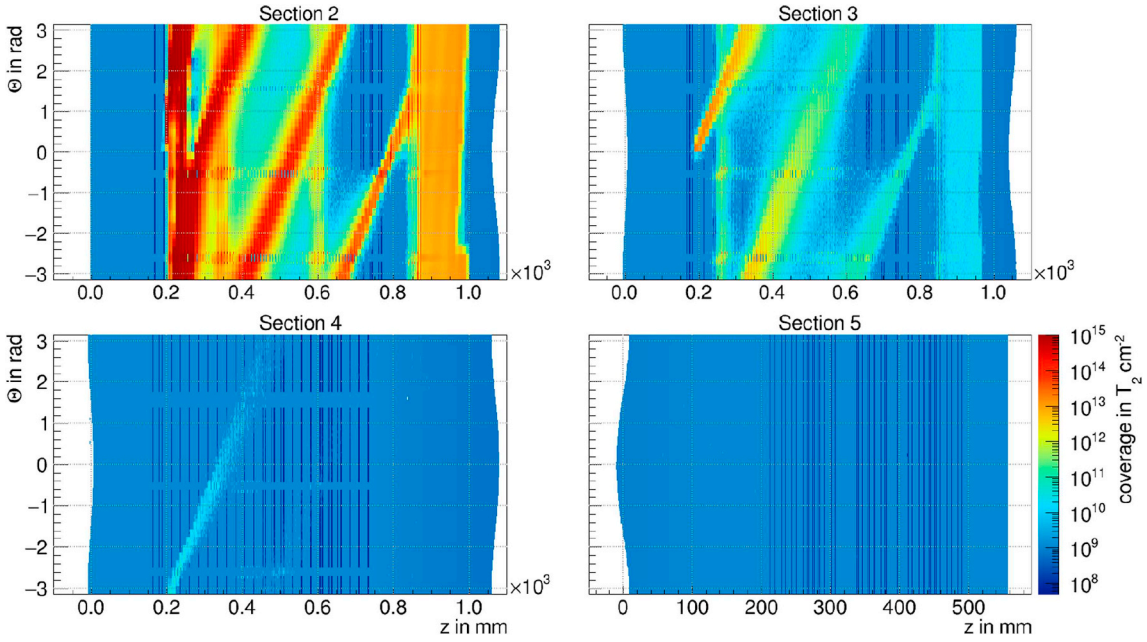

Fig. 11. Two-dimensional representation of the tritium coverage after a pumping time of 60 days, simulated with the Semi-Analytical Tracking Model. The z axis follows the central axis of the beam tube. The azimuthal angle Θ covers the full circumference of the beam tube. The apparent inhomogeneities are due to the inhomogeneous temperature profile along the cryogenic pumping section.

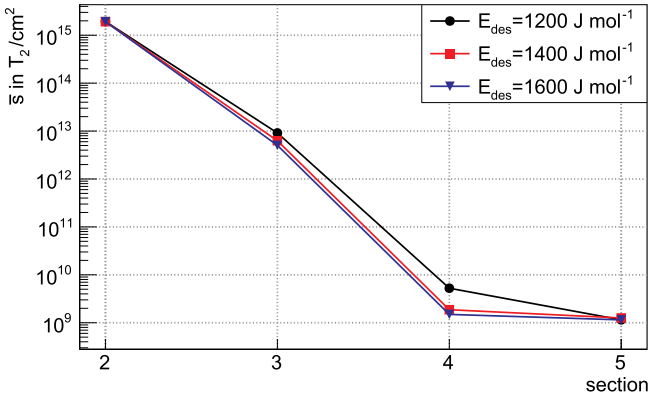

Fig. 12. Distribution of the mean surface coverage $\bar{s}$ per beam tube along the CPS, simulated with the Semi-Analytical Tracking Model. It shows an almost exponential decrease. The values for segment 5 have to be seen as an upper limit. Despite the huge number of 2.5×10^{11} simulated molecules for each setting, no significant amount of molecules reached this section.

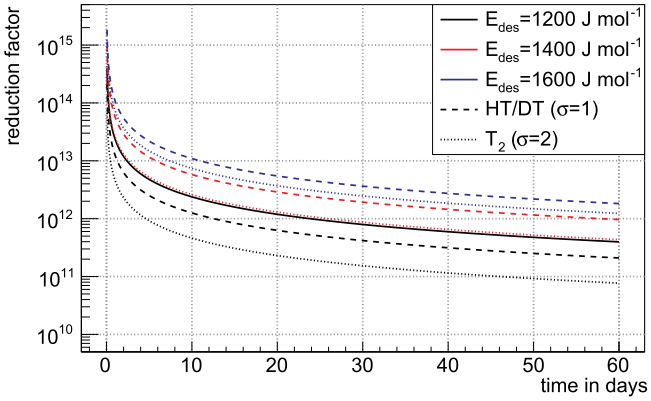

Fig. 13. Time-dependent tritium reduction when assuming no radioactivity for a desorption energy of 1200 J mol^{-1} (solid line) and for the case of a tritiated adsorbate for even higher desorption energies (dashed/dotted lines), simulated with the Semi-Analytical Tracking Model. The composition of the adsorbate is described with the variable σ which is 1 for HT/DT and 2 for pure T_2.

simulations, such as the temperature-dependent sojourn time of tritium on the argon frost layer, and the additional effect of β-decay-induced desorption, leads to an uncertainty of several orders of magnitude for the CPS reduction factor. These two effects also result in a time-dependent decline of R_{CPS}, when the desorbing gas particles slowly migrate along the pressure gradient towards the spectrometer section. However, even the most conservative assumptions for a lower limit of the reduction factor ($R_{CPS} > 10^{11}$) result in a value at least four orders of magnitude above the design value of 10^7. The combined total reduction factor of $R > 2 \times 10^{19}$ between the WGTS and the spectrometer section is more than five orders of magnitude above the initial design value of 10^{14}.

In order to retrieve more accurate parameters, measurements of the reduction of deuterium will be compared to simulations of the pressure ratios close to the inlet and outlet flanges of the pumping sections. The simulations are essential to infer the actual flow reduction factors from the measured pressure ratios. The preliminary results of the ongoing measurements with deuterium support the findings of these simulations. Further measurements and detailed comparisons with the models will help us to reduce the uncertainties of the input parameters, which would ultimately lead to more accurate predictions.

Table 2
Overview of the simulation results of the reduction factors for different isotopologues after 60 days, simulated with the Semi-Analytical Tracking Model. The reduction factors marked with a star are extrapolated values with a lower limit of 2.5×10^{11}.

E_{des} in J mol^{-1}	H_2/D_2	HT/DT	T_2
1200	$4.0 \times 10^{11*}$	2.1×10^{11}	7.7×10^{10}
1400	–	$9.6 \times 10^{11*}$	$4.3 \times 10^{11*}$
1600	–	$1.8 \times 10^{12*}$	$1.2 \times 10^{12*}$

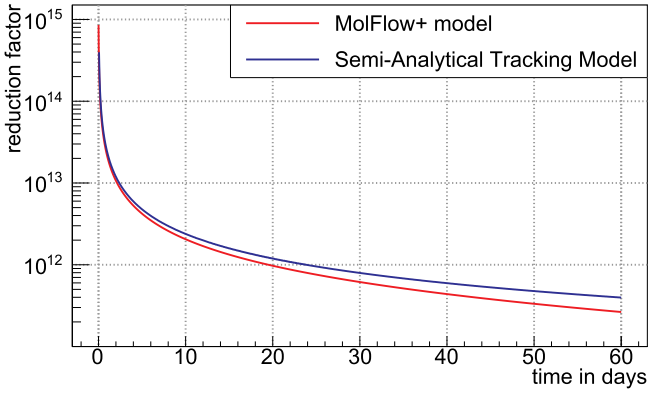

Fig. 14. CPS reduction factor results on an absolute time scale for $\alpha = 0.7$ and $E_{\mathrm{des}} = 1200$ J mol^{-1}. Both the MolFlow+ model and the Semi-Analytical Tracking Model are shown for comparison.

Acknowledgements

We acknowledge the support of the Helmholtz Association (HGF), the German Ministry for Education and Research BMBF (05A17VK2), the Helmholtz Alliance for Astroparticle Physics (HAP), the Helmholtz Young Investigator Group VH-NG-1055, the Research Training Group (GRK1694), and the DFG graduate school KSETA (GSC 1085).

References

[1] KATRIN collaboration, KATRIN design report, FZKA scientific report 7090, http://bibliothek.fzk.de/zb/berichte/FZKA7090.pdf, (2005).
[2] G. Drexlin, V. Hannen, S. Mertens, C. Weinheimer, Current direct neutrino mass experiments, Adv. High Energy Phys. (2013), https://doi.org/10.1155/2013/293986.
[3] M. Babutzka, M. Bahr, J. Bonn, B. Bornschein, A. Dieter, G. Drexlin, K. Eitel, S. Fischer, F. Glück, S. Grohmann, M. Hötzel, T. James, W. Käfer, M. Leber, B. Monreal, F. Priester, M. Röllig, M. Schlösser, U. Schmitt, F. Sharipov, M. Steidl, M. Sturm, H. Telle, N. Titov, Monitoring of the operating parameters of the KATRIN windowless gaseous tritium source, New J. Phys. 14 (10) (2012) 103046, https://doi.org/10.1088/1367-2630/14/10/103046.
[4] L. Kuckert, F. Heizmann, G. Drexlin, F. Glück, M. Hötzel, M. Kleesiek, F. Sharipov, K. Valerius, Modelling of Gas Dynamical Properties of the KATRIN Tritium Source and Implications for the Neutrino Mass Measurement href, http://arxiv.org/abs/1805.05313 arXiv:1805.05313.
[5] A. Kosmider, Tritium Retention Techniques in the KATRIN Transport Section and Commissioning of its DPS2-F Cryostat, Ph.D. thesis Karlsruher Institut für Technologie (KIT), 2012, http://nbn-resolving.org/urn:nbn:de:swb:90-289595.
[6] W. Gil, J. Bonn, B. Bornschein, R. Gehring, O. Kazachenko, J. Kleinfeller, S. Putselyk, The cryogenic pumping section of the KATRIN experiment, IEEE Trans. Appl. Supercond. 20 (3) (2010) 316–319, https://doi.org/10.1109/TASC.2009.2038581.
[7] A. Jansen, The Cryogenic Pumping Section of the KATRIN Experiment - Design Studies and Experiments for the Commissioning, Ph.D. thesis Karlsruher Institut für Technologie (KIT), 2015, http://nbn-resolving.org/urn:nbn:de:swb:90-471467.
[8] M. Ady, R. Kersevan, MOLFLOW+, Molecular Flow TPMC Simulation Code, Tech. Rep, CERN, 2016, http://molflow.web.cern.ch/.
[9] X. Luo, C. Day, V. Hauer, O. Malyshev, R. Reid, F. Sharipov, Monte Carlo simulation of gas flow through the KATRIN DPS2-F differential pumping system, Vacuum 80 (8) (2006) 864–869, https://doi.org/10.1016/j.vacuum.2005.11.044.
[10] O.B. Malyshev, Characterisation of turbo-molecular pumps by a minimum of parameters, Vacuum 81 (6) (2007) 752–758, https://doi.org/10.1016/j.vacuum.2005.11.055.
[11] M. Arenz, et al., The KATRIN superconducting magnets: overview and first performance results href, http://arxiv.org/abs/1806.08312 arXiv:1806.08312.
[12] J. Wolf, B. Bornschein, G. Drexlin, R. Gehring, R. Größle, S. Horn, N. Kernert, S. Riegel, R. Neeb, A. Wagner, Investigation of turbo-molecular pumps in strong magnetic fields, Vacuum 86 (4) (2011) 361–369, https://doi.org/10.1016/j.vacuum.2011.07.063.
[13] K. Jousten, Handbook of Vacuum Technology, John Wiley & Sons, 2008.
[14] J.D. Boer, Adsorption Phenomena, Vol. 8 of Advances in Catalysis, Academic Press, 1956, pp. 17–161 https://doi.org/10.1016/S0360-0564(08)60538-6 http://www.sciencedirect.com/science/article/pii/S0360056408605386.
[15] C. Röttele, Results of the first cool-down of the KATRIN cryogenic pumping section, J. Phys. Conf. 888 (1) (2017) 012228, , https://doi.org/10.1088/1742-6596/888/1/012228.
[16] R. Kersevan, J.-L. Pons, Introduction to MOLFLOW+: new graphical processing unit-based Monte Carlo code for simulating molecular flows and for calculating angular coefficients in the compute unified device architecture environment, J. Vac. Sci. Technol. 27 (4) (2009) 1017–1023, https://doi.org/10.1116/1.3153280.
[17] V.B. Yuferov, P.M. Kobzev, Investigation of cryosorption extraction of helium, hydrogen, and deuterium by layers of condensed gases, Sov. Phys. Tech. Phys. 14 (1970) 1261.
[18] R. Kersevan, M. Ady, Molflow+ user guide, http://molflow.web.cern.ch/, (2014).
[19] X. Luo, C. Day, Test particle Monte Carlo study of the cryogenic pumping system of the Karlsruhe Tritium Neutrino experiment, J. Vac. Sci. Technol.: Vac. Surface. Films 26 (5) (2008) 1319–1325, https://doi.org/10.1116/1.2956628.
[20] O.B. Malyshev, Tritium migration along the cryopumping section, J. Vac. Sci. Technol.: Vac. Surface. Films 26 (1) (2008) 68, https://doi.org/10.1116/1.2816945.
[21] J. Greenwood, The correct and incorrect generation of a cosine distribution of scattered particles for Monte-Carlo modelling of vacuum systems, Vacuum 67 (2) (2002) 217222, https://doi.org/10.1016/s0042-207x(02)00173-2.